

An accurate dynamical model of induction generator utilized in wind energy systems

Bilal Abdullah Nasir

Electrical Technologies Department, Hawijah Technical Institute, Northern Technical University, Kirkuk, Iraq

Article Info

Article history:

Received Dec 19, 2021

Revised Jun 14, 2022

Accepted Jul 4, 2022

Keywords:

Cross-coupling magnetizing saturation

Excitation-capacitance

Self-excited induction generator

Voltage-frequency regulation

Wind turbine

ABSTRACT

Due to the advantages of a self-excited induction generator (SEIG), it plays a main role in sources of renewable energy, such as wind turbines (WT). The regulation of terminal voltage and frequency is poor under variable rotor speed and load conditions at stand-alone operation mode. The generator terminal voltage depends on the excitation capacitance which can be controlled by a capacitor bank and static voltage compensator. The dynamical model of the machine is described by differential equations in D-Q axes transformations of the synchronously rotating frame. Many models of analysis are proposed in the literature. In those models, several approximations are used to simplify the process of calculations, such as neglecting the iron core resistance, stray load resistance, stator and rotor leakage reactance, and magnetic saturation. In this work, a comprehensive dynamic model of the SEIG-WT is performed to analyze the system performance under transient and steady-state conditions. This dynamic model considers the effect of all machine parameters variation. New analytical formulas are used for to accurate calculation of minimum and maximum values of excitation capacitance and generator rotor cut-off and maximum speed. The dynamic model results are partially compared with experimental results, and accurate agreement is shown.

This is an open access article under the [CC BY-SA](#) license.



Corresponding Author:

Bilal Abdullah Nasir

Electrical Technologies Department, Hawijah Technical Institute, Northern Technical University

AlMinsaa St, Mosul City, Nineveh Governorate, Iraq

Email: bilalalnasir@ntu.edu.iq

1. INTRODUCTION

Due to the brushless construction of a self-excited induction generator (SEIG), it is also known as brushless asynchronous generator (BAG). This generator is a good candidate with the wind turbine for electric power generation, especially in an isolated and remote area as a stand-alone generation system with a self-excitation by a capacitors bank with the following advantages; brush-less construction, it can be excited without an extra power supply, easy to parallel operation, high reliability, and efficiency, no hunting, simple construction, and operation, it has a low unit cost, low running cost, low capital cost, ruggedness and robustness construction, better transient performance, absence of moving contacts, it has no DC power supply for field excitation, and low maintenance requirements.

Although these are preferable features, induction generators have poor voltage and frequency adjusting on the generator terminal phases with the variation of load and speed. When the SEIG is directly connected to the national grid, it starts generating power when its shaft speed higher than the synchronous speed, which is limited by the grid frequency. The poor regulation of generator frequency may be adjusted by the speed-governor of the prime-mover. The blade pitch angle controller with the actuator adjusts shaft speed in the case of the SEIG-WT system. Generator terminal voltages can be regulated by excitation capacitances.

The stand-alone self-excited induction generator-wind turbine (SEIG-WT) system in an isolated mode of operation is shown in Figure 1. It consists of four components: wind turbine (prime-mover), SEIG, Excitation capacitor bank, and load. The reactive power supplied to the load is obtained by subtracting the reactive power consumed by the generator from the reactive power generated by the excitation capacitance, while the active load power equals the generated real power.

Various dynamic models of SEIG analysis have been presented by researchers [1]-[7]. In all of these models, the cross-coupling saturation of magnetizing inductance, the dynamic saturation of leakage inductances, the influence of magnetic saturation on the iron core, friction, and windage resistance, and the stray load loss resistance are neglected, which leads to un-accurate results of those models.

The present paper deals with dynamic modeling and simulation of stand-alone SEIG-WT that drove the system to feed an isolated area. The modeling of SEIG is synchronously rotating due to the voltages and currents being balanced. The dynamic magnetic saturation of magnetizing inductance, cross-coupling magnetic saturation of the magnetizing inductance, and the dynamic saturation of leakage inductances are considered in the dynamic model of the SEIG for the first time. Also, for the first time, the iron-core resistance and mechanical resistance are taken in the dynamic model in terms of air-gap magnetizing voltage by a polynomial curve fitting technique of the experimental setup measurements. The stray load loss resistance is considered in the model from measurements of the poly-phase induction machines [8]. Also, a new and simple method is used for the first time to calculate the minimum and maximum excitation capacitances, minimum and maximum speed and minimum and maximum slip of the SEIG based on the complete parameters of the generator, taking the effect of the saturated iron core and stray load loss resistances into consideration.

The wind turbine dynamic model and simulation are adopted in this paper taking wind speed and blade pitch angle of the turbine as the main variables in the model. The results of the SEIG-WT simulation of the dynamic model are partially compared with experimental setup results to show the validity of the proposed model of the system. A variable speed, separately excited DC motor is emulated of the wind turbine, and the details of the parameters are given in the appendix.

Finally, the paper is divided into six sections. Section one introduces the SEIG-WT system in the stand-alone and isolated mode of operation. Section two deals with the proposed equivalent circuit construction to derive the SEIG dynamical model including the standard tests to determine the equivalent circuit parameters of the SEIG for accurate modeling and analysis, taking the effect of saturation on the magnetizing inductance, leakage inductances, iron core resistance, and mechanical resistance. Also, this section deals with the effect of saturation on the cross-coupling magnetizing inductance and the effect of stray load loss resistance to perform a complete dynamic model of SEIG. Section three develops a simple and accurate analytical model for calculating the minimum and maximum excitation capacitance and generator rotor speed as well as slip at maximum torque.

Section four deals with the wind-turbine dynamic model based on wind speed and turbine-blade pitch angle as the main variable parameters in the model. Finally, section five adopts the main results of the SEIG-WT model by comparison to these results with experimental results, and section six gives the main conclusions.

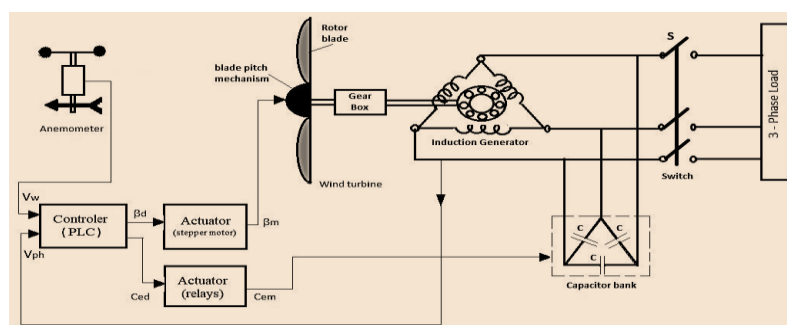


Figure 1. SEIG-WT system

2. DYNAMIC MODELING OF SEIG

To complete the dynamic model of the SEIG, the model parameters must be measured or determined from the machine proposed equivalent circuit by performing the standard test on the machine, and the machine performance can be calculated at any load conditions without actually loading it. The effect

of machine inductance saturation on the iron core and mechanical losses are considered in the model. The effect of stray load loss on the machine efficiency is also considered in the dynamic model. The effect of cross-coupling magnetizing saturation on the machine performance is also considered in the dynamic model.

2.1. Standard tests of the SEIG

To model and analyze the SEIG, the parameters of its performance must be known at any load conditions, which are obtained from standard tests such as no-load, blocked rotor, DC resistance, and no-load at synchronous speed test. A setup approach has been adopted for the calculation of stator and rotor phase resistances, stray load loss resistance, unsaturated magnetizing and leakage inductances, unsaturated iron core resistance, unsaturated mechanical loss resistance, and the saturated magnetizing inductance, leakage inductances, iron core resistance, and mechanical (friction & windage) loss resistance. The dynamically saturated components of the equivalent circuit depend on the magnetic material type of stator and rotor iron cores. All the saturated inductances depend on the magnetizing current, while the saturated iron core resistance and mechanical resistance depend on the magnetizing air gap voltage. Figure 2 shows the complete equivalent-circuit components of SEIG, the equivalent-circuit parameters are given in the appendix.

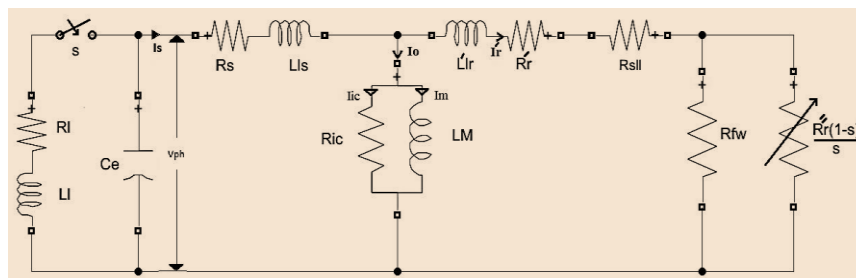


Figure 2. The proposed SEIG equivalent circuit takes the effect of stray and mechanical losses

2.2. Taking the effect of magnetizing and leakage inductance's dynamic saturation in the model

The classical linear analytical model under the assumption of fixed or linear variation of the magnetic inductances leads to unrealistic results from the dynamic model due to the model failing to take the effect of saturation in both magnetizing and leakage inductances. Indeed, the nonlinearity due to the saturation effect is of crucial importance in the case of SEIG operation and performance, due to the narrow air gap of the machine, which leads to a non-negligible saturation effect.

Therefore, for the high accuracy of simulation results, the iron core magnetic saturation and its nonlinearity have to be considered in the dynamic model simulation. In the model of SEIG, the dynamic saturation in magnetizing inductance and leakage inductances are the main factors for the stabilization and starting up of the generated terminal voltage. Hence, the inclusion of these inductance variations with magnetizing current and machine load current must be implemented in the dynamic model.

Analytical expressions of magnetizing and leakage inductances from their practical relations with magnetizing and load currents, and a polynomial curve fitting technique are employed in Matlab, and the estimated functions are obtained as (1) to (3):

$$L_M = 0.04765 * I_m^5 - 0.5129 * I_m^4 + 2.18 * I_m^3 - 4.57 * I_m^2 + 4.636 * I_m + 0.25 \tag{1}$$

$$L_{\ell s} = 4.824 * 10^{-5} * I_{ph}^5 - 0.000714 * I_{ph}^4 + 0.00414 * I_{ph}^3 - 0.01174 * I_{ph}^2 + 0.0159 I_{ph} + 0.0156 \tag{2}$$

$$\dot{L}_{\ell r} = 5.27 * 10^{-5} * I_{ph}^5 - 0.0008987 * I_{ph}^4 + 0.00577 * I_{ph}^3 - 0.0176 * I_{ph}^2 + 0.0251 * I_{ph} + 0.023 \tag{3}$$

by storing these functions in the Matlab Simulink of the dynamic model, the values of the saturated inductances can be updated at each step of integration.

2.3. Magnetic saturation effect on the iron core and mechanical losses

Nonlinearity in the iron core and mechanical resistances due to the saturation of the magnetic core can be taken into the SEIG model to increase the accuracy of simulation results. This condition is also

necessary for studying the voltage build-up in the isolated mode of SEIG operation since the linear model is not able of studying the performance of such systems.

In general, the actual non-linearity in iron core and mechanical loss resistances can be found from the no-load test to assess the SEIG performance during the loading. Iron core resistance (R_{ic}) and mechanical loss resistance (R_{fw}) exhibit variations, but overall the iron-core resistance decrease with increasing air-gap magnetizing voltage while the mechanical loss resistance increases with increasing air gap voltage. Any change in load, speed, or excitation-capacitance will change the degree of saturation in the iron core, which consecutively will change values of R_{ic} and R_{fw} , resulting in variable iron core and mechanical losses. These two resistances are determined experimentally at synchronous speed and modeled by the polynomial curve fitting as (4) and (5):

$$R_{ic} = -0.0001985 * V_g^3 + 0.111 * V_g^2 - 23.11 * V_g + 840 \quad (4)$$

$$R_{fw} = -6.167 * V_g^4 + 0.00419 * V_g^3 - 1.074 * V_g^2 + 127.4 * V_g + 560 \quad (5)$$

the air gap magnetizing voltage (V_g) can be calculated by adding the stator voltage drop in the stator impedance to the stator terminal voltage.

2.4. Stray load loss resistance model

To complete the dynamic model of SEIG for accurate performance calculations from the simulation results, all the losses determination must be considered in the model. This loss is represented by resistance ($R_{s\ell\ell}$) inserted in the SEIG equivalent circuit as shown in Figure 2. This component is connected in series with the rotor resistance (\hat{R}_r). Calculation of the stray load loss resistance requires performing a test at the rated full load, no-load, and the variable load of the machine. This loss is approximated by 1.8% of full load output machine power for small and medium-size machines and the stray load resistance can be calculated as [9].

$$R_{s\ell\ell} = 0.018 * \hat{R}_r * (1 - S_m) / S_m \quad (6)$$

Where \hat{R}_r is the rotor resistance reflected on the stator side? S_m is the full load slip at maximum torque and determined from the equivalent circuit components as will be shown later due to the minimum and maximum of SEIG excitation capacitance and speed depending on this slip. The physical representation and evaluation of stray load losses is a controversial and difficult problem in electrical machinery. IEEE 112-B Standard represents these losses by a parasitic resistance connected in series with rotor resistance in the rotor branch of the equivalent circuit, as shown in Figure 2. It follows that the stray loss depends on the square of the rotor current and the machine's full load slip. From the proposed equivalent circuit, the load resistance $\hat{R}_r(1 - s) / s$ is derived as (7).

$$\hat{R}_r(1 - s) / s = 1 / \left[1 / \left\{ \frac{\hat{R}_r(1-s)}{s} - R_{s\ell\ell} \right\} - \frac{1}{R_{fw}} \right] \quad (7)$$

2.5. Cross-coupling magnetizing saturation

The progress in the PWM technique, inverter-fed induction generator as voltage and frequency regulator as well as operation of an induction generator in isolated power system have led to an increase in the possibilities of including the mutual or magnetizing and leakage fluxes saturation effect in the dynamic model of SEIG. The saturation effect in the main flux of induction machines introduces a cross-coupling magnetizing saturation effect that is not predicted by the non-linear dependency magnetizing and leakage inductances modeling. The cross-coupling saturation is assumed to be entirely in the magnetizing inductance. Hence different models have been developed to obtain differential equations for analyzing the cross saturation effect [10]-[12]. In all of these models, the stator-constant reference frame model is utilized for analyzing the effect of cross-coupling magnetizing saturation, except in [10] the model cannot be solved due to it has six unknowns and four differential equations only.

The curve of saturated magnetizing inductance is required to determine the static magnetizing inductance L_m and the dynamic magnetizing inductance (L_{my}). This curve is determined by the no-load test of the machine at synchronous speed for a variable supply voltage from 25% to 125%. At this test, the air gap voltage (V_g), the static magnetizing inductance (L_M), dynamic magnetizing inductance L_{My} , and the cross-coupling magnetizing inductance (L_{Mdq}) are determined as [11]:

$$V_g = V_{ph} - I_s * (R_s + jX_{\ell s}) \tag{8}$$

$$L_M = f(i_m) = \frac{V_g}{\omega_s i_m} = \frac{\lambda_m}{i_m} \tag{9}$$

$$L_{My} = \frac{d\lambda_m}{di_m} = L_M + |i_m| * \frac{dL_M}{d|i_m|} \tag{10}$$

$$L_{Mdq} = L_{Mqd} = \frac{i_{md} * i_{mq}}{|i_m|} * \frac{dL_M}{di_m} \tag{11}$$

where V_{ph} is the machine terminal voltage (V).

I_s is the machine terminal current (A).

R_s is the stator resistance per phase (Ω).

$X_{\ell s}$ is the stator leakage reactance per phase (Ω).

λ_m is the magnetizing flux linkage per phase.

The magnetizing current (i_m) has real and imaginary components (i_{md} and i_{mq}) and can be given as (12).

$$i_m = i_{md} + j i_{mq}, |i_m| = \sqrt{i_{md}^2 + i_{mq}^2} \tag{12}$$

The components of the magnetizing inductance (L_M) are L_{Md} and L_{Mq} and can be given as (13) and (14).

$$L_{Md} = L_M + \frac{i_{md}}{i_{mq}} * L_{Mdq} = L_M + \frac{L_{Md}^2}{i_m} * \frac{dL_M}{di_m} \tag{13}$$

$$L_{Mq} = L_M + \frac{i_{mq}}{i_{md}} * L_{Mdq} = L_M + \frac{L_{Mq}^2}{i_m} * \frac{dL_M}{di_m} \tag{14}$$

Also the components of the air gap voltage (V_g) per phase can be derived as (15) to (17).

$$V_{gd} = \frac{d\lambda_{md}}{dt} = L_{Mdq} * \frac{di_{mq}}{dt} + L_{Md} * \frac{di_{md}}{dt} = \omega_s * (L_{Md} * i_{md} + L_{Mdq} * i_{mq}) \tag{15}$$

$$V_{gq} = \frac{d\lambda_{mq}}{dt} = L_{Mdq} * \frac{di_{md}}{dt} + L_{Mq} * \frac{di_{mq}}{dt} = \omega_s * (L_{Mq} * i_{mq} + L_{Mdq} * i_{md}) \tag{16}$$

$$V_g = \sqrt{V_{gd}^2 + V_{gq}^2} \tag{17}$$

Where λ_{md} , λ_{mq} , V_{gd} and V_{gq} are the D-Q axes components of magnetic flux linkage and magnetizing air gap voltage per phase respectively. ω_s is the angular frequency (rad/sec).

2.6. Modified equivalent circuits of SEIG

The iron core loss is normally modeled as equivalent resistance (R_{ic}) that represents the power dissipated in the core identified practically from the no-load test. If the iron core loss is inserted in a dynamic model of the machine, a sixth-order model will be obtained. By appropriate modification of the parallel core resistance into serial equivalent resistance in the stator circuit, the dynamic model is reduced to the fourth-order model. The parallel branch can be modified into a series equivalent magnetizing inductance (L_m) and iron core resistance (R_{ics}). These series components of the parallel branch are calculated as (18) and (19).

$$L_m = \frac{L_M * R_{ic}^2}{[R_{ic}^2 + (\omega_s L_M)^2]} \tag{18}$$

$$R_{ics} = \frac{R_{ic} * (\omega_s L_M)^2}{[R_{ic}^2 + (\omega_s L_M)^2]} \tag{19}$$

Where ω_s = the voltage angular speed (rad/sec).

The series iron core resistance in the parallel branch (R_{ics}) is reflected in the stator side as a series voltage drop with an equivalent stator circuit, as shown in Figure 3, and can be calculated as (20).

$$V_{ds} = R_{ics} * I_m \tag{20}$$

This modified equivalent circuit of SEIG is a preferable model due to taking main and leakage magnetic flux saturation and iron core loss determination without increasing the model order.

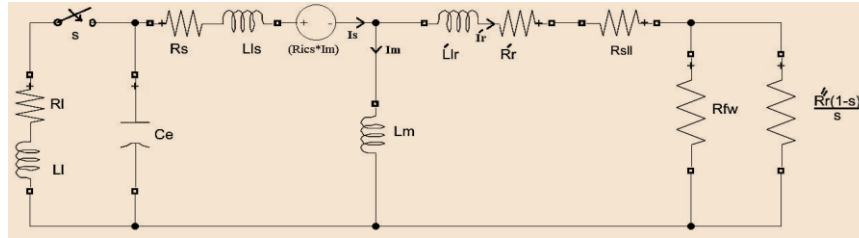


Figure 3. Modified the proposed equivalent circuit of SEIG with reflection iron core resistance on the stator circuit

2.7. Complete dynamic model of SEIG

Modified equivalent circuit of SEIG in synchronously rotating reference frame as shown in Figure 4. The 3-phase machine can be analyzed by an equivalent two-phase machine with Park's transformation [4], [10]. Both stator and rotor parameters are transformed into a synchronously rotating reference frame that moves with a rotating magnetic field. This model is very important and preferred for transient analysis and will be used in the present dynamic model of SEIG analysis by choosing the electrical machine currents as the main variables in the model. Figure 4(a) and Figure 4(b) show the D and Q axes equivalent circuit model of SEIG with excitation-capacitance, stray load loss resistance, and inductive load in a synchronously rotating frame of the stator and rotor parameters.

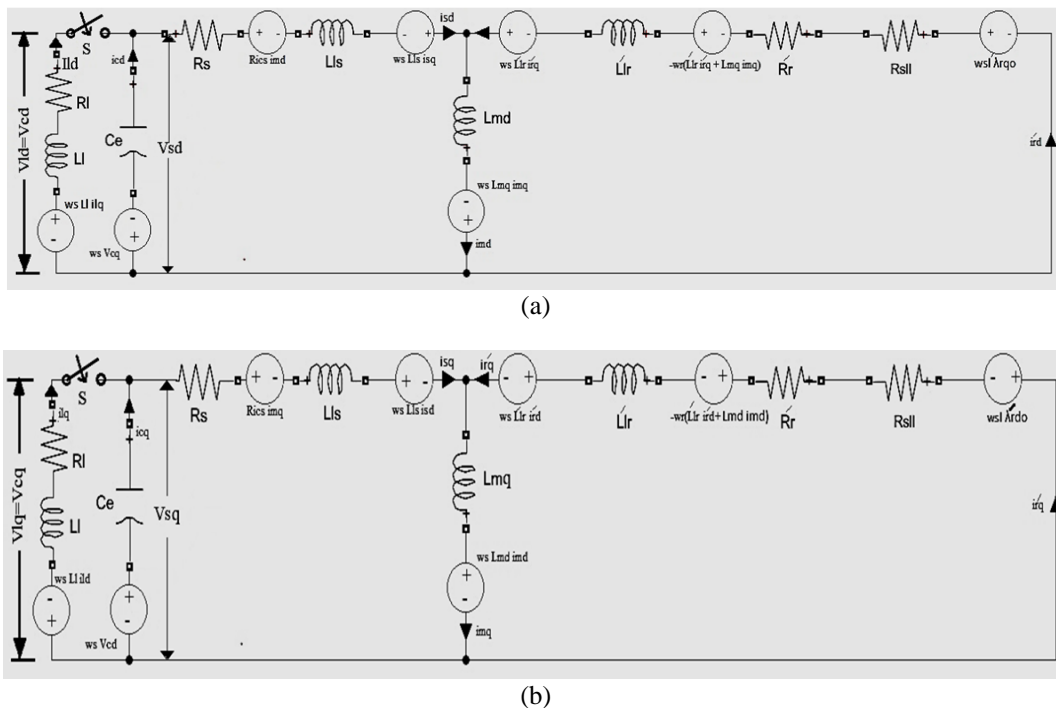


Figure 4. Modified equivalent circuit of SEIG in synchronously rotating reference frame, (a) D-axis model, and (b) Q-axis model

From the model, the stator and rotor voltages at no load taking the cross-coupling magnetizing saturation are obtained as (21) to (30):

$$v_{sd} = R_s * i_{sd} + L_{\ell s} * \frac{di_{sd}}{dt} + R_{ics} * i_{md} - \omega_s * L_{\ell s} * i_{sq} + \frac{d\lambda_{md}}{dt} - \omega_s * L_{mq} * i_{mq} \quad (21)$$

$$v_{sq} = R_s * i_{sq} + L_{\ell s} * \frac{di_{sq}}{dt} + R_{ics} * i_{mq} + \omega_s * L_{\ell s} * i_{sd} + \frac{d\lambda_{mq}}{dt} + \omega_s * L_{md} * i_{md} \quad (22)$$

$$v_{rd} = 0 = (\hat{R}_r + R_{s\ell\ell}) * i_{rd} + \hat{L}_{\ell r} * \frac{i_{rd}}{dt} - \omega_{s\ell} * (\hat{L}_{\ell r} * i_{rq} + L_{mq} * i_{mq}) + \frac{d\lambda_{md}}{dt} - \omega_{s\ell} * \hat{\lambda}_{rq0} \quad (23)$$

$$v_{rq} = 0 = (\hat{R}_r + R_{s\ell\ell}) * i_{rq} + \hat{L}_{\ell r} * \frac{i_{rq}}{dt} + \omega_{s\ell} * (\hat{L}_{\ell r} * i_{rd} + L_{md} * i_{md}) + \frac{d\lambda_{mq}}{dt} + \omega_{s\ell} * \hat{\lambda}_{rd0} \quad (24)$$

$$\frac{d\lambda_{md}}{dt} = L_{mdq} * \frac{di_{mq}}{dt} + L_{md} * \frac{di_{md}}{dt} \text{ D- axis flux linkage} \quad (25)$$

$$\frac{d\lambda_{mq}}{dt} = L_{mdq} * \frac{di_{md}}{dt} + L_{mq} * \frac{di_{mq}}{dt} \text{ Q- axis flux linkage} \quad (26)$$

$$L_{mdq} = \frac{i_{md} * i_{mq}}{|i_m|} * \frac{dL_m}{di_m} \text{ cross-coupling inductance} \quad (27)$$

$$i_{md} = (i_{sd} + i_{rd}) \text{ D- axis current} \quad (28)$$

$$i_{mq} = (i_{sq} + i_{rq}) \text{ Q- axis current} \quad (29)$$

$$\omega_{s\ell} = (\omega_s - \omega_r) \text{ slip speed in rad/sec} \quad (30)$$

Where ω_r is the generator shaft speed in electrical radian/sec.
 L_{md} and L_{mq} are D-and Q-axes components of magnetizing inductance.

$$\text{Let } L_d = L_{sd} * L_{rd} - L_{md}^2 \quad (31)$$

$$L_q = L_{sq} * L_{rq} - L_{mq}^2 \quad (32)$$

where $L_{sd} = L_{\ell s} + L_{md}$ D- axis stator self-inductance.

$L_{rd} = \hat{L}_{\ell r} + L_{md}$ D-axis rotor self-inductance.

$L_{sq} = L_{\ell s} + L_{mq}$ Q-axis stator self-inductance.

$L_{rq} = \hat{L}_{\ell r} + L_{mq}$ Q-axis rotor self-inductance.

Then substitute (25), (26), (31), and (32) into (21) to (24) and re-arrange these equations as a function of stator and rotor currents, the following four first-order differential equations can be obtained:

$$\frac{di_{sd}}{dt} = \frac{L_{rd}}{L_d} * [v_{sd} - (R_s + R_{ics}) * i_{sd} - R_{ics} * i_{rd} + \omega_s (L_{sq} * i_{sq} + L_{mq} * i_{rq})] - \frac{L_{md}}{L_d} [- (\hat{R}_r + R_{s\ell\ell}) i_{rd} + \omega_{s\ell} (L_{rq} * i_{rq} + L_{mq} * i_{sq} + \hat{\lambda}_{rq0})] - \frac{L_{\ell r}}{L_d} * L_{mdq} * \omega_s * i_{mq} \dots \quad (33)$$

$$\frac{di_{sq}}{dt} = \frac{L_{rq}}{L_q} * [v_{sq} - (R_s + R_{ics}) * i_{sq} - R_{ics} * i_{rq} - \omega_s (L_{sd} * i_{sd} + L_{md} * i_{rd})] - \frac{L_{mq}}{L_q} [- (R_r + R_{s\ell\ell}) i_{rq} - \omega_{s\ell} (L_{rd} * i_{rd} + L_{md} * i_{sd} + \hat{\lambda}_{rd0})] - \frac{L_{\ell r}}{L_q} * L_{mdq} * \omega_s * i_{md} \dots \quad (34)$$

$$\frac{di_{rd}}{dt} = \frac{L_{sd}}{L_d} * [- (\hat{R}_r + R_{s\ell\ell}) i_{rd} + \omega_{s\ell} (L_{rq} * i_{rq} + L_{mq} * i_{sq} + \hat{\lambda}_{rq0})] - \frac{L_{md}}{L_d} \left[\begin{matrix} v_{sd} - \\ (R_s + R_{ics}) * i_{sd} + \omega_s (L_{sq} * i_{sq} + L_{mq} * i_{rq}) - R_{ics} * i_{rd} \end{matrix} \right] - \frac{L_{\ell s}}{L_d} * L_{mdq} * \omega_s * i_{mq} \dots \quad (35)$$

$$\frac{di_{rq}}{dt} = \frac{L_{sq}}{L_q} * [- (\hat{R}_r + R_{s\ell\ell}) i_{rq} - \omega_{s\ell} (L_{rd} * i_{rd} + L_{md} * i_{sd} + \hat{\lambda}_{rd0})] - \frac{L_{mq}}{L_q} \left[\begin{matrix} v_{sq} - \\ (R_s + R_{ics}) * i_{sq} - \omega_s (L_{sd} * i_{sd} + L_{md} * i_{rd}) - R_{ics} * i_{rq} \end{matrix} \right] - \frac{L_{\ell s}}{L_q} * L_{mdq} * \omega_s * i_{md} \dots \quad (36)$$

The differential (33) to (36) are fed directly to the Matlab Simulink Block-set as a current space model to solve the first-order differential equations of the SEIG D-Q model without the need for matrix inversion in each step of integration as in conventional state-space models. The following auxiliary differential equations are used to complete the solution of the dynamic model of SEIG. The stator phase voltage components in the D and Q axes (v_{sd} and v_{sq}) is calculated as a function of excitation-capacitance voltage in the D and Q axes (v_{cd} and v_{cq}) as (37) and (38):

$$v_{sd} = -v_{cd} = \int \left(\frac{i_{cd}}{C_e} + \omega_s * v_{cq} \right) dt + V_{cd0} \quad (37)$$

$$v_{sq} = -v_{cq} = \int \left(\frac{i_{cq}}{C_e} - \omega_s * v_{cd} \right) dt + V_{cq0} \quad (38)$$

where $i_{cd} = i_{sd} - i_{ld}$ D-axis capacitance current component.

$i_{cq} = i_{sq} - i_{lq}$ Q-axis capacitance current component.

i_{ld} and i_{lq} are the D-and-Q axes load current components calculated from the following differential equations in case of the resistive-inductive load:

$$\frac{di_{ld}}{dt} = \frac{1}{L_\ell} * (v_{ld} - R_\ell * i_{ld}) + \omega_s * i_{lq} \quad (39)$$

$$\frac{di_{lq}}{dt} = \frac{1}{L_\ell} * (v_{lq} - R_\ell * i_{lq}) - \omega_s * i_{ld} \quad (40)$$

Where v_{ld} and v_{lq} are the load voltage D-Q components and can be calculated as (41):

$$v_{ld} = v_{cd}, v_{lq} = v_{cq} \quad (41)$$

R_ℓ is the resistive component of the load and L_ℓ is the inductive component of the load.

Then the generated electro-magnetic torque inside the machine (T_e) can be calculated as (42):

$$T_e = \left(\frac{3}{2} \right) * (P_p) * (L_m) * (i_{sd} * i_{rq} - i_{sq} * i_{rd}) \quad (42)$$

Where P_p = the machine number of pole pairs.

The angular frequency of the generated terminal voltage is to be calculated as (43):

$$\omega_s = i_{cq} / (C_e * v_{sd}) \quad (43)$$

The D-Q components of the stator flux linkage are to be calculated as (44) and (45):

$$\lambda_{sd} = \int (v_{sd} - i_{sd} * R_s) . dt \quad (44)$$

$$\lambda_{sq} = \int (v_{sq} - i_{sq} * R_s) . dt \quad (45)$$

The maximum stator phase voltage and current can be determined as (46) and (47):

$$V_{ph(m)} = \sqrt{v_{sd}^2 + v_{sq}^2} \quad (46)$$

$$I_{ph(m)} = \sqrt{i_{sd}^2 + i_{sq}^2} \quad (47)$$

The active load power is given as (48):

$$P_\ell = \frac{3}{2} * [v_{sd} * i_{ld} + v_{sq} * i_{lq}] \quad (48)$$

The total apparent power of the machine is calculated as (49):

$$S_t = \frac{3}{2} * V_{ph(m)} * I_{ph(m)} \tag{49}$$

The load power factor can be calculated as (50):

$$\cos\phi_\ell = P_\ell / S_t \tag{50}$$

3. MINIMUM AND MAXIMUM SEIG SPEED AND EXCITATION VALUES IN STAND-ALONE OPERATION

For calculation of the suitable value of the critical capacitor to initiate the SEIG-WT system successfully, many calculation methods are proposed in the literature [13]-[24].

The methods of excitation capacitors calculation, mentioned in the above literature are used inconvenient models with several approximations to simplify the steps of the calculation, such as a limited range of speed and resistive load, neglecting the iron core resistance, the stray load loss resistance, and the effect of magnetizing saturation. Also, most of the previous works use a numerical iteration method to determine the minimum and maximum excitation capacitance, but the iteration procedure takes a long time, and maybe a divergence occurs, and this process cannot be used online.

The section contains a new, simple, and accurate analytical procedure that depends on the equivalent circuit parameters of the machine to determine the critical (minimum and maximum) excitation capacitor and critical (minimum and maximum) generator rotor speed values. The theoretical results from the proposed formulas are compared with experimental results, using the parameters of the induction generator configured in the laboratory to show the validity of the new method. The excitation-capacitance calculation is based on the resonance between the stator winding inductance and excitation capacitance at no load. Selecting the resonance frequency equals the machine base frequency at no load. The formula for calculation of excitation capacitance can be derived as (51):

$$C_e = \frac{1}{\omega_r^2 \cdot (L_m + L_{\ell s})} \tag{51}$$

In all literature, the authors have used this equation for determining the minimum excitation capacitance which is not a true assumption, the minimum and maximum excitation capacitance depend on the maximum and minimum generator rotor speed (ω_r) in electrical radian/sec. These minimum and maximum excitation capacitances are calculated as (52) and (53):

$$C_{e(max)} = \frac{1}{\omega_{rc}^2 \cdot (L_m + L_{\ell s})} \tag{52}$$

$$C_{e(min)} = \frac{1}{\omega_{rm}^2 \cdot (L_m + L_{\ell s})} \tag{53}$$

Where ω_{rc} = the cut-off or minimum rotor speed in (electrical rad/sec).

ω_{rm} is the maximum (above synchronous speed) allowable machine speed in electrical radian/second

$$\omega_{rc} = \omega_s \cdot (1 - S_m) \tag{54}$$

$$\omega_{rm} = \omega_s \cdot (1 + S_m) \tag{55}$$

where ω_s = the angular-frequency in electrical. rad/sec.

S_m = the slips at maximum torque. The slip is positive when the machine rotates under synchronous speed, and it is negative when the machine rotates above synchronous speed.

The slip at maximum torque is calculated from the machine equivalent circuit analysis, taking the effect of iron core resistance (R_{ic}) and stray load loss resistance ($R_{s\ell\ell}$) as well as the dynamic saturation into account. By applying Thevenin's theorem on the proposed circuit in Figure 2, the following relations are obtained:

$$R_{tht} = \frac{[R_{ic} \cdot X_{thm}^2 + R_{ic} \cdot R_{thm} \cdot (R_{ic} + R_{thm})]}{[(R_{ic} + R_{thm})^2 + X_{thm}^2]} \tag{56}$$

$$X_{tht} = \frac{R_{ic}^2 \cdot X_{thm}}{[(R_{thm} + R_{ic})^2 + X_{thm}^2]} \tag{57}$$

Where R_{tht} = the total of the Thevenin's equivalent resistance of the circuit.

X_{tht} = the total of Thevenin's equivalent reactance.

R_{thm} = the Thevenin's equivalent circuit resistance and is determined as (58):

$$R_{thm} = \frac{R_s \cdot X_m^2}{[R_s^2 + (X_{\ell s} + X_m)^2]} \quad (58)$$

X_{thm} is the Thevenin's equivalent reactance taking the effect of magnetizing inductance only, and is calculated as (59):

$$X_{thm} = \frac{X_m \cdot [R_s^2 + X_{\ell s} \cdot (X_{\ell s} + X_m)]}{[R_s^2 + (X_{\ell s} + X_m)^2]} \quad (59)$$

The maximum torque of the machine occurs at maximum power transfer between the stator and rotor, and this condition will occur when the rotor resistance component (R_r/s) equal to the other components of the circuit as (60):

$$\frac{R_r}{s} = R_{tht} + R_{s\ell\ell} + j(X_{tht} + X_{\ell r}) \quad (60)$$

The slip at maximum torque is obtained as (61):

$$S_m = \dot{R}_r / [(R_{tht} + R_{s\ell\ell})^2 + (X_{tht} + X_{\ell r})^2]^{1/2} \quad (61)$$

For approximation results, if the magnetizing inductance and iron core resistance are neglected the slip at maximum torque becomes (62):

$$S_m = \dot{R}_r / [(R_s + R_{s\ell\ell})^2 + (X_{\ell s} + X_{\ell r})^2]^{1/2} \quad (62)$$

4. THE TURBINE-GENERATOR DYNAMIC MODEL

The wind turbine is modeled by relations of power coefficient (C_p) as a function of both tip speed ratio (λ) and blade pitch angle (β). The value of λ is fixed at its maximum values, and the power coefficient (C_p) will become maximum also. The tip speed ratio is the ratio of angular turbine rotor speed to linear wind speed at the tip of turbine blades [25], [26]. It can be given as (63):

$$\lambda = \omega_t \cdot R / V_\omega \quad (63)$$

R is the blade length. V_ω is the speed of wind in (m/s) and ω_t is the shaft speed in mechanical rad/second. The swept wind power in Watt is calculated as (64):

$$P_\omega = \frac{1}{2} \cdot \rho_a \cdot A \cdot V_\omega^3 \quad (64)$$

Where ρ_a is the air-specific density in (K_g/m^3).

A is the swept area by the blades in (m^2).

The turbine output power (P_t) can be calculated as (65):

$$P_t = C_p \cdot P_\omega \quad (65)$$

The turbine torque in (N.m) can be written as (66):

$$T_t = C_t \cdot P_\omega \quad (66)$$

Where C_t is the torque coefficient and given as (67):

$$C_t = C_p / \lambda \quad (67)$$

A suitable way to control the power obtained by the wind turbine is to adjust the blade pitch angle (β). The blade pitch is similar to the gate valve in hydroelectric power turbines, except that its response is

much faster. At a downwind speed ($V_\omega \leq 13 \text{ m/s}$), the value of β is fixed at approximately Zero degrees and not required to be adjusted, while the turbine operates at maximum power. If the wind speed becomes greater than 13 m/s , the turbine power will highly increase due to it being increased with cubic wind speed, and it must be adjusted by controlling the blade pitch angle to prevent the turbine from destruction.

The controller will feed the required or demand β (β_d) to the actuator, and the actuator (stepper motor) will adjust the required pitch angle to reduce the turbine speed and power at fixed rate values. For a realistic actuator response to the pitch angle, the actuator uses the time constant integrator, so that the pitch angle is from 0° to 20° with a rate of change $\mp 1^\circ$ per second. The actuator can be modeled as (68) [27]:

$$\beta = \frac{1}{\tau_\beta} \cdot \int (\beta_d - \beta_m) dt \tag{68}$$

Where β_m is the measured pitch angle by the actuator and τ_β is the actuator time constant in deg/sec? The power coefficient (C_p) in terms of tip speed ratio (λ) and the turbine blade pitch angle (β) in degree is obtained as (69):

$$C_{p(\lambda,\beta)} = C_1 * \left[\frac{C_2}{\lambda_i} - C_3 \cdot \beta - C_4 \right] * e^{\left(\frac{-C_5}{\lambda_i} \right)} + C_6 \cdot \lambda, \lambda_i = \left[\frac{0.08 \cdot \beta^4 + \lambda \cdot \beta^3 + 0.08 \cdot \beta + \lambda}{\beta^3 - 2.8 \cdot 10^{-3} \cdot \beta - 0.035 \cdot \lambda + 1} \right] \tag{69}$$

where $C_1 = 0.5176$, $C_2 = 116$, $C_3 = 0.4$, $C_4 = 5$, $C_5 = 21$ and $C_6 = 0.0068$

The generator shaft speed in (electrical. rad/sec) can be calculated by integrating the first-order differential equation of the motion as (70):

$$\frac{d\omega_r}{dt} = \frac{P_p}{J} * (T_{sh} - T_e - D * \omega_m) \tag{70}$$

Where ω_m is the generator shaft speed in (mechanical rad/sec) and can be calculated as (71):

$$\omega_m = \omega_r / P_p \tag{71}$$

where J is the total inertia of the turbine-generator system in ($K_g \cdot m^2$), and calculated as (72):

$$J = \left(\frac{J_t}{G^2} + J_g \right) \tag{72}$$

where J_t is wind turbine moment of inertia and J_g is the generator moment of inertia, and can be obtained from the deceleration (retardation) test. G is the gear-box ratio and can be obtained as (73):

$$G = \frac{\omega_m}{\omega_t} = \frac{T_t}{T_{sh}} \tag{73}$$

T_{sh} is the torque on the generator rotor (load torque) in N.m developed by the turbine and can be calculated as (74):

$$T_{sh} = \frac{T_t}{G} \tag{74}$$

Where T_t is the aerodynamic torque of the turbine shaft and can be calculated as (75):

$$T_t = P_t / \omega_t \tag{75}$$

D is the viscous friction torque coefficient in [$N \cdot m / (rad./sec.)$] and can be calculated as (76) [28]-[30]:

$$D = P_{f\omega} / \omega_m^2 \tag{76}$$

Where: $P_{f\omega}$ is the mechanical power loss.

T_e is the generator electromagnetic torque calculated by equation (42)?

5. RESULTS AND DISCUSSION

In the experimental setup, a 3-phase, squirrel cage, 220V, Δ - connected induction machine is joined to a wind turbine and acts as a prime-mover. Test results and simulation results in Matlab/Simulink of the

SEIG-WT system are presented at no load initiation of the self-excitation. The SEIG is driven at 1525 r.p.m (above synchronous speed). Then a connected delta excitation capacitance bank of $40 \mu F$ was switched across the SEIG stator terminals. The induction machine and wind turbine specifications and parameters are given as:

SEIG specifications and equivalent circuit parameters:

3-phase, squirrel cage rotor, 220 V, 50 Hz, Δ - Connected with the following parameters:

$$P_{out} = 1500 W, I_\ell = 6.6 A, N_s = 1500 r.p.m, \cos \Phi = 0.8, P_p = 2, J_g = 0.03 K_g.m^2$$

$$D = 0.003 N.m/(Rad./sec.), C_{ex(min)} = 30 \mu F, R_s = 5.1 \Omega, R_r = 3.5 \Omega, \text{Cut-off speed} = 1200 r.p.m$$

Design class B, Insulation class-F

Wind turbine specifications:

$$P_{out(max)} = 1750 W, \text{Blades} = 3, \rho_a = 1.225 \frac{Kg}{m^3}, C_{p(max)} = 0.4, R = 1m (\text{radius}), G = 1.25 (\text{gear ratio}).$$

Variations in magnetizing inductance and stator and rotor leakage inductances as the main influencing parameters have been considered into account by the experimental non-linear relationships between magnetizing-inductance and current and between leakage inductances and load current as in (1) to (3). Variations in iron core and mechanical resistances are taken into account by experimental non-linear relations between these resistances and air gap magnetizing voltage as given in (4) and (5). Building-generator terminal voltage as shown in Figure 5. Variation of permissible cut-off and maximum rotor speed has been tested experimentally, as a parameter to the generated voltage and calculated analytically by (54) and (55). Figure 5(a) and Figure 5(b) show the experimental and MATLAB simulation results for starting-generator terminal voltage under transient conditions.

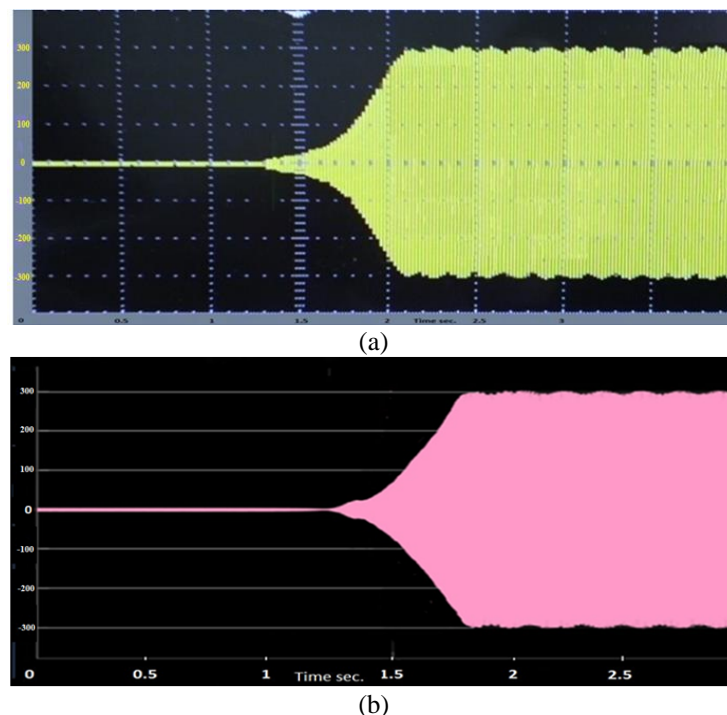


Figure 5. Building-generator terminal voltage, (a) experimental result and (b) MATLAB simulation result

Building-generator terminal voltage as shown in Figure 6. From these figures, it can be shown that very good agreement between the experimental results and theoretical simulation due to the accurate simulation model, which considers into account all the SEIG-WT system parameters and variables. Figure 6(a) and Figure 6(b) show the experimental and Matlab simulation results of the steady-state terminal voltage of the generator. Figure 7 shows the MATLAB result of the electromagnetic torque of the generator at starting-up conditions.

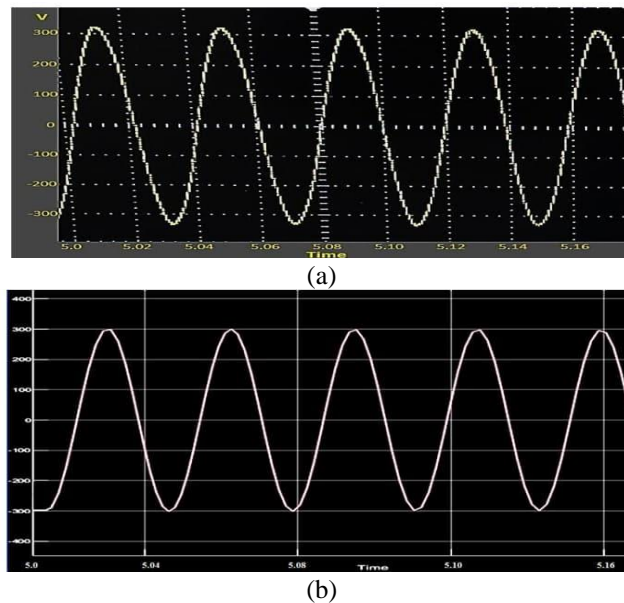


Figure 6. Steady-state generator phase voltage, (a) experimental result and (b) MATLAB simulation result

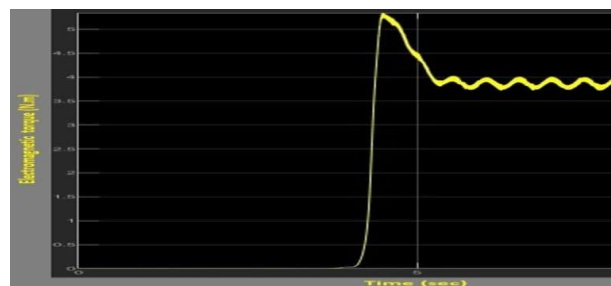


Figure 7. Matlab simulation results of electromagnetic torque of SEIG during the starting-up condition

6. CONCLUSION

In this dynamic model of the SEIG-WT system, all important parameters of SEIG are considered without introducing extra differential equations to the model, due to the modification in the equivalent circuit of SEIG. The dynamic saturation of magnetizing-inductance, cross-coupling magnetizing-inductance, and leakage-inductances are taken in the model due to these parameters are the main variables that influence the SEIG performance in steady-state as well as transient conditions. The influence of magnetizing saturation of the air-gap voltage on the iron core loss and mechanical loss, as well as the influence of stray load loss, are considered in the dynamic model for accurate prediction of the system performance. New, simple, and accurate analytical formulas are derived for the calculation of minimum and maximum excitation capacitances and rotor speed of SEIG. These formulas are obtained from the comprehensive equivalent circuit of the machine and based on maximum power transfer theory.





REFERENCES

- [1] T. Ouchbel *et al.*, "Regulation of the reactive excitation power of the asynchronous wind turbine at variable speed," *Journal of Smart Grid and Renewable Energy*, vol. 4, no. 3, pp. 272-280, 2013, doi: 10.4236/sgre.2013.43033.
- [2] D. Chermiti, N. Abid, and A. Khedher, "Voltage regulation approach to a self-excited induction generator: Theoretical study and experimental validation," *International Transactions on Electrical Energy Systems*, vol. 27, no. 5, pp. 1-11, 2016, 10.1002/etep.2311.
- [3] B. Palle, M. G. Simoes, and F. A. Farret, "Dynamic simulation and analysis of parallel self-excited induction generators for the islanded wind farm system," *IEEE Transactions on Industry Applications*, vol. 41, no. 4, pp. 1099-1106, 2005, doi: 10.1109/TIA.2005.851040.
- [4] A. Kishore and G. S. Kumar, "Dynamic modeling and analysis of three-phase self-excited induction generator using the generalized state-space approach," *International Symposium on Power Electronics, Electrical Drives, Automation and Motion (SPEED AM)*, 2006, pp. 1459-1466, doi: 10.1109/SPEEDAM.2006.1649998.
- [5] K. Idjdarene, D. Rekioua, T. Rekioua, and A. Tounzi, "Control strategies for an autonomous induction generator taking the saturation effect into account," *Energy Conversion and Management*, vol. 49, no. 10, 2008, doi: 10.1016/j.enconman.2008.05.014.

- [6] T. Ouchbel, S. Zouggar, M. Sedik, M. Oukili, M. Alhafyani, and A. Rabhi, "Control of the reactive excitation power of asynchronous wind turbine with variable speed," *International Renewable Energy Congress*, 2020, pp. 242-249.
- [7] A. Upasana and Y. Kumsuwan, "Closed-loop speed control of induction generator with scalar control inverters," *Energy procedia*, Elsevier Publisher, vol. 34, pp. 371-381, 2013, doi: 10.1016/i.egypro.2013.06.765.
- [8] B. A. Nasir, "Stray loss estimation in induction motor," *International Journal of Electrical Engineering and Technology (IJEET)*, vol. 12, no. 11, pp. 19-25, 2021, doi: 10.34218/IJEET.12.11.2021.002
- [9] "IEEE standard test procedure for polyphase induction motors and generators," in *IEEE Standard-112-1991*, 1991, doi: 10.1109/IEEESTD.1991.114383.
- [10] M. Imadouchene, "Transient analysis of the self-excited induction generator subjected to grid disturbances," *TELKOMNIKA Indonesian Journal of Electrical engineering*, vol. 16, no. 2, pp. 199-206, 2015, doi: 10.11591/tjee.v16i2.1604.
- [11] P. Pillay, V. Levin, P. Otaduy, and J. Kueck, "In-Situ induction motor efficiency determination using the genetic algorithm," *IEEE Transactions on Energy Conversion*, vol. 13, no. 4, pp. 326-333, December 1998, doi: 10.1109/60.736318.
- [12] K. E. Hallenius, P. Vas, and J. E. Brown, "The analysis of a saturated self-excited asynchronous generator," *IEEE Transactions on Energy Conversion*, vol. 6, no. 2, pp. 336-345, 1991, doi: 10.1109/60.79641.
- [13] R. S. Khela and K. S. Sandhu, "ANN model for estimation of capacitance requirements to maintain constant air gap voltage of self-excited induction generator with variables load," *International Journal of Computer Science and Technology*, vol. 2, no. 4, pp. 53-57, 2011.
- [14] S. Kumar, S. Pradhan, and R. N. Sahu, "Excitation capacitance requirements of three-phase self-excited induction generator for windmill application," *2013 International Conference on Energy Efficient Technologies for Sustainability*, 2013, pp. 365-370, doi: 10.1109/ICEETS.2013.6533410.
- [15] A. Abbo, M. Barara, A. Ouchatti, M. Akherraz, and H. Mahmoudi, "Capacitance required analysis for self-excited induction generator," *Journal of Theoretical Applications and Applied Information Technology*, vol. 55, no. 3, pp. 382-389, 2013.
- [16] A. K. Mohanty, and K. B. Yadav, "Estimation of excitation capacitance requirement of an isolated multi-phase induction generator for power generation," *International Journal of Power Electronics and Drive System (IJPEDS)*, vol. 7, no. 2, pp. 561-567, 2016, doi: 10.11591/ijpeds.v7.i2.pp561-567.
- [17] T. Mhamdi, A. Barhoumi, and L. Sbita, "Stand-alone self-excited induction generator driven by a wind turbine," *Alexandria Engineering Journal*, vol. 57, no. 2, pp. 781-786, 2018, doi: 10.1016/j.aej.2017.01.009.
- [18] D. Chermiiti and A. Khedher, "Two reliable approaches to determine the critical excitation capacitor value for a SEIG operating in stand-alone," *2017 International Conference on Green Energy Conversion Systems (GECS)*, 2017, pp. 1-6, doi: 10.1109/GECS.2017.8066155.
- [19] A. Sharma and G. Kaur, "Assessment of capacitance for self-excited induction generator in sustaining constant air-gap voltage under variable speed and load," *Energies*, vol.11, no. 10, pp. 2- 16, Sep. 2018, doi: 10.3390/en11102509.
- [20] S. Rajakaruna and R. Bonert, "A technique for the steady-state analysis of a self-excited induction generator with variable speed," *IEEE Transactions on Energy Conversion*, vol. 8, no. 4, pp. 757-761, Dec. 1993, doi: 10.1109/60.260991.
- [21] L. Shridhar, B. Singh, C. S. Jha, B. P. Singh, and S. S. Murthy, "Selection of capacitors for the self-regulated short shunt self-excited induction generator," in *IEEE Transactions on Energy Conversion*, vol. 10, no. 1, pp. 10-17, 1995, doi: 10.1109/60.372563.
- [22] K. A. Nigam, M. M. A. Salama, and M. Kazerani, "Identifying machine parameters influencing the operation of the self-excited induction generator," *Electric Power System Research*, vol. 69, no. 2-3, pp. 123-128, 2004, doi: 10.1016/j.epsr.2003.08.003.
- [23] M. Bodson and O. Kiselychynk, "Analytic conditions for spontaneous self-excitation in induction generators," *Proceedings of the 2010 American Control Conference*, 2010, pp. 2527-2532, doi: 10.1109/ACC.2010.5530579.
- [24] V. Sankardoss, S. P. Sabberwal, and K. Rajambal, "Experimental design of capacitance required for self-excited induction generator," *Journal of Theoretical and Applied Information Technology*, vol. 45, no. 1, pp. 1-8, 2012.
- [25] S. Khajuria and J. Kaur, "Implementation of pitch control of wind turbine using Simulink (Matlab)," *International Journal of Advanced Research in Computer Engineering and Technology*, vol. 1, no. 4, pp. 196-200, 2012.
- [26] S. Pal and D. Jana, "Pitch angle control of variable speed wind turbine generation," *International Journal of Electrical Engineering and Technology (IJEET)*, vol. 5, no. 3, pp. 69-80, 2014.
- [27] C. Eisenhut, F. Krug, and C. Schram, "Wind turbine model for system simulation near cut-in wind speed," *IEEE Transactions on Energy Conversion*, vol. 22, no. 2, pp. 414-420, June 2007, doi: 10.1109/TEC.2006.875473.
- [28] M. B. Sigrid, "Modeling and analysis of variable-speed wind turbines with induction generator during grid fault," Ph.D. Dissertation, Institute of Energy Technology, Aalborg University, Denmark, 2004.
- [29] B. A. Nasir, "Theory and design of traveling wave induction heaters for flat metallic workpieces," Ph.D. Dissertation, AL - Mustansiriyah University, Baghdad, Iraq, 1997.
- [30] H. Chen and C. Bi, "Optimal starting frequency of three-phase induction motor," *IET Electric Power Applications*, vol. 16, pp. 62-69, Nov. 2021, doi: 10.1049/elp2.12159.

BIOGRAPHIES OF AUTHORS



Bilal Abdullah Nasir     was born in 1958, in Iraq. He received a B.Sc. of Electrical Engineering from the University of Technology, Baghdad-Iraq, 1980, an M.Sc. of Electrical Engineering (Power & Machines) from the University of Mosul, Iraq, in 1984, and a Ph.D. of Electrical engineering (Power & Machines) from Al-Mustansiriyah University, Iraq, in 1997. He has been employed as a lecturer at Northern Technical University, Iraq/Hawijah Technical Institute, Kirkuk, Iraq from 1988 up to date. Now he was an Assistant Professor in Electrical power systems and Machines. He can be contacted at email: bilalalnasir@ntu.edu.iq.